Brillouin scattering study of elastic properties in ferroelectric copolymer single-crystalline films

Leo Otani and Akira Yoshihara
School of Science and Engineering, Ishinomaki Senshu University, Ishinomaki 986-8580, Japan

Hiroji Ohigashi
Department of Polymer Science and Engineering, Yamagata University, Yonezawa 992-8510, Japan
(Received 1 March 2001; published 19 October 2001)

The in-plane elastic properties of as-grown random copolymer poly (vinylidene fluoride–trifluoroethylene) single-crystalline films with 75/25 molecular ratio have been studied by Brillouin light scattering up to $\sim 140\,^{\circ}\mathrm{C}$ from room temperature, covering the D_{6h}-C_{2v} ferroelectric phase transition at $\sim 126\,^{\circ}\mathrm{C}$. The in-plane longitudinal acoustic (LA) phonons propagating parallel and perpendicular to the polymer chains were examined. In spite of the strongly first-order nature of the phase transition, both LA velocities exhibit only a broad down step in the temperature range between $\sim 100\,^{\circ}\mathrm{C}$ and $\sim 130\,^{\circ}\mathrm{C}$, depending on the propagation direction, with increasing temperature. The LA phonon width perpendicular to the polymer chains increases with increasing temperature, and exhibits a broad maximum centered at $\sim 120\,^{\circ}\mathrm{C}$. On the other hand, the LA phonon width along the polymer-chain axis is much wider than the width perpendicular to the polymer chains, and continues to increase even in the paraelectric phase. Treating the E_u symmetry electric polarizations (P_x, P_y) of the D_{6h} point group as the macroscopic order parameter, a Laudau free energy was developed to discuss the elastic properties. Using the free energy, we found that the elastic anomalies expected through the electrostrictive couplings between the order parameter and the elastic strains are strongly suppressed by the intrinsic electrical nature of the ferroelectric polymer. For both LA phonons, the temperature development of the phonon frequency and width can be reasonably reproduced by the Cole-Davidson relaxation model for the velocity dispersion with an exponent of $\beta_{\mathrm{CD}}=0.4$. The relaxation time was found to obey the Arrhenius law $\tau=\tau_0 \exp(\Delta E/k_{\mathrm{B}}T)$ with $\Delta E=0.55\pm 0.01$ eV and $\tau_0=(4.0\pm 0.6)\times 10^{-18}$ s. At $24.0\,^{\circ}\mathrm{C}$ in the ferroelectric phase, the in-plane phonon width anisotropy can be reasonably described by $\gamma_{\mathrm{B}}(\theta)/2\pi=0.18+0.72\sin^4\theta$ for the LA phonon and $\gamma_{\mathrm{B}}(\theta)/2\pi=0.02+0.095\sin^2 2\theta$ for the transverse acoustic phonon, where the phonon propagation angle θ is measured from the perpendicular direction with respect to the polymer-chain axis. The θ dependence is strongly related to the one-dimensional freedom constrained in each copolymer chain.

DOI: 10.1103/PhysRevE.64.051804 PACS number(s): 82.35.Lr, 78.35.+c, 77.80.Bh, 77.84.Jd

I. INTRODUCTION

Polyvinylidene fluoride (PVDF) has been known as a unique polymer material with strong piezoelectric and pyroelectric activities since the late 1960s. In 1974, the ferroelectricity of PVDF was confirmed by the observation of a D-E hysteresis loop in this organic polymer material [1]. However, the expected paraelectric-ferroelectric phase transition (PFPT) has not been detected below the melting temperature. Random copolymers consisting of vinylidene fluoride and trifluoroethylene, P[VDF/TrFE], have been found to be ferroelectric polymers and undergo a PFPT below the melting temperature [2]. Because of their strong piezoelectric and pyroelectric activities, suitable for many industrial applications, the physical properties of P[VDF/TrFE] films have been intensively investigated [3,4]. The PFPT is first order and accompanied by a large thermal hysteresis in the PFPT temperature T_{c}. It is considered to be an order-disorder transition between the dynamically disordered polymer chains predominantly composed of *trans-gauche-trans-gauche′* ($TGTG'$) sequences with partly *trans-trans* (TT) sequences above T_{c} and all *trans* (TT) chains below T_{c}. Since the PFPT is strongly correlated with the rearrangements of the intrachain conformations as well as the interchain configurations, it is important to prepare single-crystal films with 100% crystallinity and free from lamellar structure for understanding of the microscopic mechanism of the PFPT. However, preparation of single-crystal films was difficult in practice.

Recent improvements of crystallization techniques for P[VDF/TrFE] copolymer films by Ohigashi and co-workers made it possible to prepare highly ordered single-crystalline (SC) P[VDF/TrFE] films with 75/25 molecular ratio, which hereafter we abbreviate as SC 75/25 films, with almost 100% crystallinity and free from lamellar structure [5,6]. In their SC 75/25 films, spontaneous polarization appears perpendicular to the polymer chains aligned within the film plane, but is inclined $\pm 30\,^{\circ}$ from the surface normal under $(30–80)\times 10^6$ V/m of poling electric field [5]. Because of the ferroelectric twin structure, the films are not perfect single-crystal films, but SC or twinned films. Ohigashi and co-workers have investigated the physical properties of SC 75/25 films using a variety of experimental techniques including piezoelectric resonance [5], dielectric spectroscopy [6,7], x-ray diffraction (XRD) [7], electro-optical spectroscopy [8,9], and shear velocity measurements [7]. The PFPT occurs at $T_{\mathrm{c}}\sim 127\,^{\circ}\mathrm{C}$ during heating and $T_{\mathrm{c}}\sim 78\,^{\circ}\mathrm{C}$ upon cooling, and the SC 75/25 film melts at $T_{\mathrm{m}}\sim 149\,^{\circ}\mathrm{C}$ [6,7]. XRD results indicate that the polymer chains are arranged in a honeycomb structure with D_{6h} symmetry across the film above T_{c} [5]. The sixfold axis coincides with the polymer-chain direction within the film plane. Below T_{c} the honey-

comb arrangement of the polymer chains is slightly distorted into a base-centered orthorhombic arrangement with C_{2v} symmetry. The ferroelectric axis is the shortest *b* axis of the orthorhombic cell.

Brillouin light scattering (BLS) is the best technique to investigate the elastic properties of thin film materials, like polymer films. BLS studies of the PFPT in P[VDF/TrFE] films have been performed by Krüger and co-workers [10,11] and by Liu and Schmidt [12]. Both groups measured the sound velocity (V) of the in-plane longitudinal acoustic (LA) phonons, which propagate parallel and perpendicular to the polymer chains, as a function of temperature. According to their results, in spite of the strongly first-order nature of the PFPT, the LA velocities exhibit a broad down step around T_c as temperature increases. This behavior was attributed to a distribution of T_c within their films. Krüger *et al.* reported a similar temperature dependence and thermal hysteresis between the mass density ρ and the elastic constant $C=\rho V^2$ [11]. There is another interesting observation that the T_c values deduced from the LA velocities are different for the parallel and perpendicular directions with respect to the polymer chain [10,12]. Thus the elastic properties of P[VDF/TrFE] films near the PFPT are not fully understood.

In our previous report, we studied the in-plane elastic anisotropy of as-grown and poled SC 75/25 films by BLS at room temperature in the ferroelectric phase [13]. We analyzed the anisotropy by developing two models that take account of the ferroelectric domain orientations, and determined a set of elastic constants for each model. In order to elucidate the elastic properties of SC 75/25 films near the PFPT, we continued our BLS studies. In this report, we present the frequency and width of the in-plane LA phonons propagating parallel and perpendicular to the polymer chains as a function of temperature up to $\sim 140\,^{\circ}$C through the PFPT. We also examined the in-plane phonon width anisotropy at $24.0\,^{\circ}$C in the ferroelectric phase.

II. EXPERIMENT

SC 75/25 films with almost 100% crystallinity were prepared at the Faculty of Engineering, Yamagata University. The as-grown SC 75/25 films were provided as a long sheet 14×50 mm^2 in size along the polymer-chain direction. The details of the SC film preparation techniques were reported in Refs. [5,6]. Since as-grown and poled films are found to be elastically identical in the ferroelectric phase, at least at room temperature [13], we only examined as-grown SC films with thickness of $\sim 40\,\mu$m in this study.

The BLS studies were performed at Ishinomaki Senshu University (ISU). We employed a 90A scattering geometry which allows us to examine the in-plane acoustic phonons [13,14]. For this PFPT study, we prepared an oven suitable for the 90A scattering geometry at the machine shop of the Research Institute for Scientific Measurements (RISM), Tohoku University. With this oven we can rotate a sample holder with an accuracy of $\pm 1\,^{\circ}$ from outside the oven. The holder temperature was regulated within an accuracy of better than $\pm 0.1\,^{\circ}$C over two hours up to $160\,^{\circ}$C using a bridge regulator with a platinum resistance sensor and a proportional regulator with a differential-type copper-Constantan thermocouple (CCT) to compensate temperature difference across the holder. The holder has a hole of 3 mm in diameter with $45\,^{\circ}$ edges to accept the incident and scattered beams. The sample temperature was monitored by another CCT placed just beside the hole. The as-grown SC 75/25 sheet was cut into small pieces ($\sim 7\times 7$ mm^2) and a piece of the SC 75/25 film was placed inside the holder to ensure good thermal contact and uniformity.

Inelastically scattered light, excited by a *p*-polarized line at 532 nm from a solid state laser with power of ~ 150 mW, was analyzed using a $(3+3)$-pass tandem Fabry-Pérot interferometer (FPI) and detected by a thermoelectrically cooled photomultiplier tube followed by photon counting electronics [15]. Several FPI mirror spacings between 5 mm and 15 mm were used. In order to minimize possible local heating and damage by the laser beam near T_c, we reduced the laser output power step by step, finally to ~ 20 mW, above $120\,^{\circ}$C. In this study we always performed one-way measurements of BLS spectra during heating from room temperature. Because of lower laser power and increasing phonon width, especially for the LA phonon propagating along the polymer-chain direction, the BLS signal became very weak and typical spectrum accumulation time was over 2 h above $\sim 120\,^{\circ}$C. Since the BLS spectra became extremely poor in quality near $\sim 140\,^{\circ}$C, probably due to premelting, we stopped our measurements around this temperature.

III. RESULTS AND DISCUSSION

For the sake of convenience in the following discussion, we define the film coordinates as follows: the polymer-chain direction within a film plane is assigned to the *z* axis and the surface normal to the *x* axis, and the *y* axis is orthogonal to them and in the film plane. These film coordinates coincide with the crystallographic one's in the D_{6h} phase with the film *z* axis as the sixfold axis. Hereafter, we refer to these film coordinates.

Figure 1 shows the temperature development of the *y*-axis LA phonon spectrum. Here we make a comment. We always have a pure LA phonon along the *z* axis, which is the common *c* axis of the orthorhombic cell for every ferroelectric domain. On the other hand, for the *y* axis, we have quasiacoustic phonons in general, because of the $60\,^{\circ}$ ferroelectric domain orientations around the *z* axis [13]. Although we should distinguish a quasi-LA phonon from a pure LA phonon, we will use the term ''LA phonon'' even for the quasi-LA phonon through this report for the sake of convenience. Figure 2 shows the temperature development of the *z*-axis LA phonon spectrum. A weaker peak outside the main peak on both frequency sides is contamination due to the backscattering component that was generated by the internal reflection of the incident laser beam at the film/air interface. Since the frequency ranges displayed in Figs. 1 and 2 are adjusted to be the same, it is obvious that the *z*-axis LA phonon width is much larger than the *y*-axis LA phonon width, in spite of its pure LA phonon character.

It is obvious from Figs. 1 and 2 that the phonon width increases with increasing temperature for both LA phonons.

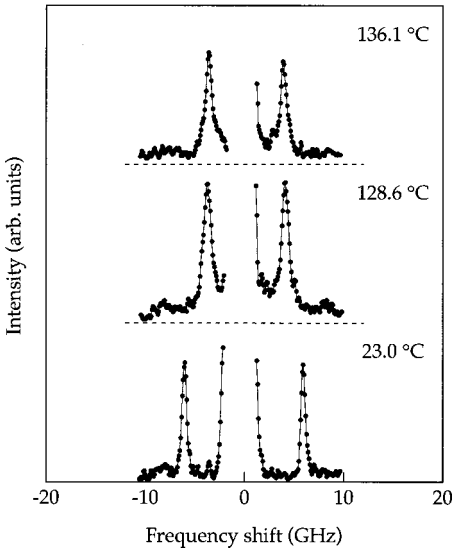

FIG. 1. Temperature development of BLS spectra due to the *y*-axis LA phonon. BLS spectra within a frequency range of ± 20 GHz are displayed for comparison with the *z*-axis spectra displayed in Fig. 2 below. The temperature is indicated on each spectrum. The broken lines show the baselines of each spectrum.

In order to determine the frequency shift ($\omega_0/2\pi$) and the width ($\gamma/2\pi$, full width at half maximum), we performed numerical convolution analyses of the spectra by assuming a damped harmonic oscillator (DHO) response function

$$S(\omega) \propto k_B T \frac{\gamma}{[\omega^2 - \omega_0^2]^2 + \omega^2 \gamma^2} \tag{1}$$

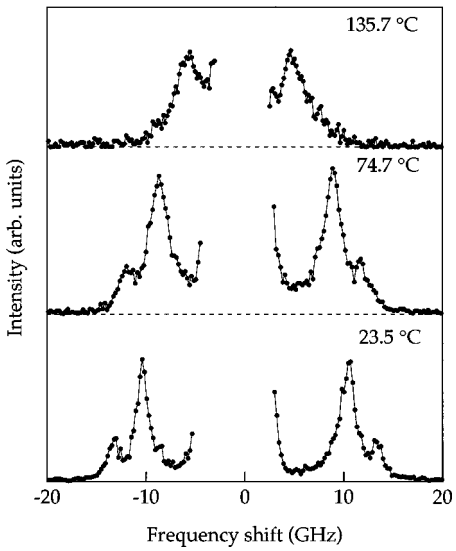

FIG. 2. Temperature development of BLS spectra due to the *z*-axis LA phonon. BLS spectra within a frequency range of ± 20 GHz are displayed. The weak higher-frequency peak outside the main peak is a contamination due to the backscattering component generated by the internal reflection of the laser beam at the film/air interface. The temperature is indicated on each spectrum. The broken lines show the baselines of each spectrum.

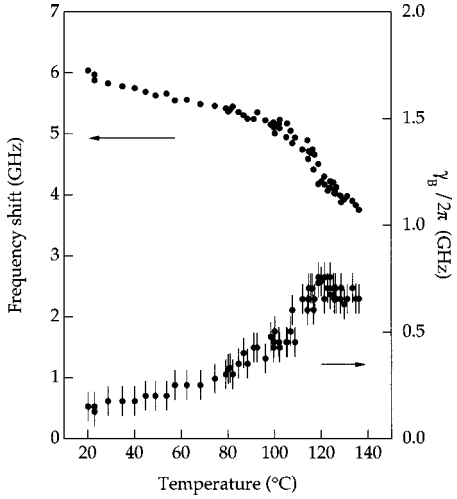

FIG. 3. The peak frequency $\Delta\nu_B$ and width $\gamma_B/2\pi$ as a function of temperature for the *y*-axis LA phonon.

for the LA phonons. We adopted the elastic Rayleigh peak as the instrumental function. The details of the convolution analysis are described in Ref. [16]. For a highly damped oscillator, like the *z*-axis LA phonon, the peak frequency ($\Delta\nu_B$) and width ($\gamma_B/2\pi$) do not coincide with the DHO values $\omega_0/2\pi$ and $\gamma/2\pi$. We need to evaluate the peak frequency and width using

$$2\pi\Delta\nu_B = (\omega_0^2 - \gamma^2/2)^{1/2} \tag{2}$$

and

$$\gamma_B = [\omega_0^2 - \gamma^2/2 + \gamma(\omega_0^2 - \gamma^2/4)^{1/2}]^{1/2} - [\omega_0^2 - \gamma^2/2 - \gamma(\omega_0^2 - \gamma^2/4)^{1/2}]^{1/2}. \tag{3}$$

Figures 3 and 4 show the peak frequency ($\Delta\nu_B$) and width ($\gamma_B/2\pi$) of the in-plane LA phonons as a function of temperature up to $\sim 140\,°C$. For each LA phonon, the peak frequency almost linearly decreases as temperature increases up

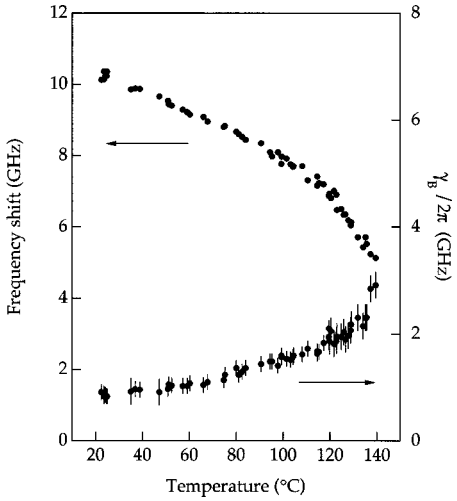

FIG. 4. The peak frequency $\Delta\nu_B$ and width $\gamma_B/2\pi$ as a function of temperature for the *z*-axis LA phonon.

to $\sim 100\,^{\circ}$C. As temperature further increases up to $\sim 140\,^{\circ}$C, a broad down step appears in the temperature range between $\sim 100\,^{\circ}$C and $\sim 130\,^{\circ}$C, depending on the propagation direction. These results are qualitatively the same as the previous results [10,11]. In the 90A scattering geometry, one can directly evaluate the sound velocity V from the obtained peak frequency through [14]

$$V = 2\pi\Delta\nu_{\mathrm{B}}/k = \lambda\Delta\nu_{\mathrm{B}}/\sqrt{2}. \tag{4}$$

Here, $\lambda(=532$ nm) is the vacuum wavelength of the laser light, and $k = 2\sqrt{2}\pi/\lambda$ is the phonon momentum. Note that the index of refraction does not appear in Eq. (4). This is the most important virtue of the 90A-scattering geometry. On the other hand, the widths behave in a quite different manner. For the *y*-axis LA phonon, the width gradually increases, and then exhibits a broad maximum centered at $\sim 120\,^{\circ}$C. However, the *z*-axis LA phonon width is unusually large even at room temperature (for example, ~ 0.9 GHz for the *z* axis and ~ 0.17 GHz for the *y* axis), and continues to increase up to $\sim 140\,^{\circ}$C. In contrast with the sharp PFPT detected by the shear velocity study [7], the PFPT detected by the BLS technique is quite obscure.

A. Landau free-energy description

In this section we discuss the elastic properties of SC 75/25 films near the PFPT using a Landau free-energy description. Although this PFPT is first order, the point groups D_{6h} and C_{2v} satisfy the group-subgroup relation. XRD and dielectric results [5,6] indicate that this PFPT occurs at the Brillouin zone center. One can then choose the doubly degenerate electric polarizations (P_x, P_y) belonging to the E_u representation of the D_{6h} point group as the macroscopic order parameter (OP) of this PFPT. Note that the polarizations are specified in the film coordinates. Of course, it is very possible that there can be a microscopic OP that describes the conformation changes within a polymer chain [17]. With the macroscopic OP and the P_z polarization component, we can construct a Landau free energy as follows [13]:

$$G_{\mathrm{P}} = \frac{1}{2\chi_z}P_z^2 + \frac{\alpha(T)}{2}(P_x^2+P_y^2) + \frac{\beta}{4}(P_x^2+P_y^2)^2 + \frac{\gamma}{6}(P_x^2+P_y^2)^3 + \frac{\delta}{2}P_y^2(P_y^2-3P_x^2)^2, \tag{5}$$

in which we assume $\chi_z > 0$, $\alpha(T) = \alpha_0(T - T_0)$, $\beta < 0$, $\gamma > 0$, $\delta < 0$, and $\gamma + 3\delta > 0$, and ignore a fourth-order term $P_x^2P_y^2$ and a sixth-order term $P_x^2(P_x^2-3P_y^2)^2$ which are not relevant in our discussion. Here, we introduce two-dimensional polar coordinates in the OP space, $P_x = P\sin\varphi$ and $P_y = P\cos\varphi$. We can then readily obtain three $120\,^{\circ}$ domains specified as follows: $\varphi = 0$ for domain I, $\varphi = 2\pi/3$ for domain II, and $\varphi = 4\pi/3$ for domain III. These domains are accompanied by their antiphase domains I′ $(\varphi = \pi)$, II′ $(\varphi = 5\pi/3)$, and III′ $(\varphi = \pi/3)$. Of course, this is equivalent to six $60\,^{\circ}$ domains specified as $\varphi = n\pi/3$ $(n = 0$–$5)$. By applying a poling electric field of $(30$–$80)\times 10^6$ V/m along the surface normal *x* axis, the domains II′ and III are converted into the domains III′ and II, and the ferroelectric twin structure with spontaneous polarizations inclined $\pm 30\,^{\circ}$ from the surface normal appears [5]. However, the in-plane domains I and I′ are not affected by the poling electric field. The $P_x^2P_y^2$ and $P_x^2(P_x^2-3P_y^2)^2$ terms introduce some distribution $\Delta\varphi$ $(= \pm 5\,^{\circ})$ [6] around the stable domain orientations.

In order to discuss the elastic properties near the PFPT, we introduce the elastic energy and the OP-strain coupling terms. The elastic energy in the D_{6h} phase is given by

$$G_{\mathrm{el}} = \frac{1}{2}\frac{C_{11}^{(0)}+C_{12}^{(0)}}{2}(e_1+e_2)^2 + \frac{1}{2}C_{33}^{(0)}e_3^2 + C_{13}^{(0)}(e_1+e_2)e_3 + \frac{1}{2}C_{44}^{(0)}(e_4^2+e_5^2) + \frac{1}{2}C_{66}^{(0)}[e_6^2+(e_1-e_2)^2]. \tag{6}$$

Here, $C_{\mathrm{ij}}^{(0)}$ stands for the bare elastic constant in the D_{6h} phase and the hexagonality condition $C_{66}^{(0)} = (C_{11}^{(0)} - C_{12}^{(0)})/2$ is satisfied. The LA phonons propagating along the *y* and *z* axes are pure LA modes in the D_{6h} phase with velocities given by $(C_{11}^{(0)}/\rho)^{1/2}$ and $(C_{33}^{(0)}/\rho)^{1/2}$, respectively. Next, we consider the OP-strain coupling terms. Taking account of symmetry properties of the elastic strains and the E_u symmetry of the OP in the D_{6h} point group, one can readily construct the OP-strain coupling terms as follows:

$$G_{\text{el-P}} = A\{2P_xP_ye_6 + (P_x^2-P_y^2)(e_1-e_2)\} + (P_x^2+P_y^2)\times\{B(e_1+e_2) + Ce_3 + D(e_4^2+e_5^2)\} + F(P_xP_ze_5 + P_yP_ze_4). \tag{7}$$

Furukawa *et al.* have shown linear relations between the induced piezoelectric constants and the spontaneous polarization in the ferroelectric C_{2v} phase [18]. The electrostrictive coupling terms between the OP and the strains in Eq. (7) result in linear relations between the induced piezoelectric constants and the spontaneous polarization.

Since our film coordinates coincide with the crystallographic coordinates for the domain I ($P_x = 0$ and $P_y = P_{\mathrm{S}}$), it is convenient to start with this domain. Here, P_{S} can be readily calculated as

$$P_{\mathrm{S}}^2 = \frac{|\beta'| + \sqrt{\beta'^2 + 4\alpha_0\gamma'(T_0-T)}}{2\gamma'} = \frac{|\beta'|}{2\gamma'}\left[1 + \sqrt{1 + \frac{4\alpha_0\gamma'}{\beta'^2}(T_0-T)}\right], \tag{8}$$

in which we assume $\gamma' = \gamma + 3\delta > 0$ and $\beta' = \beta - \Delta\beta \simeq \beta < 0$. Here, $\Delta\beta$ gives a renormalization of the fourth-order expansion coefficient in Eq. (5) through the OP-strain couplings in Eq. (7). After straightforward calculations, one obtains a set of elastic constants in both phases as summarized in Table I.

TABLE I. Compatibility of the elastic constants between the D_{6h} and C_{2v} phases. Five independent elastic constants in the D_{6h} phase split into nine independent elastic constants in the C_{2v} phase. Here, Σ and Δ are defined by $\Sigma=\beta+2\gamma' P_S^2$ and $\Delta=9|\delta|P_S^2+4A^2/C_{66}^{(0)}$. We have $\Sigma\simeq|\beta|/2$ at $T=T_c$.

Ferroelectric C_{2v} phase	Paraelectric D_{6h} phase
$C_{11}=C_{11}^{(0)}-2(A-B)^2/\Sigma$	$C_{11}^{(0)}$
$C_{22}=C_{11}^{(0)}-2(A+B)^2/\Sigma$	$C_{11}^{(0)}$
$C_{33}=C_{33}^{(0)}-2C^2/\Sigma$	$C_{33}^{(0)}$
$C_{44}=C_{44}^{(0)}+(D-F^2\chi_z)P_S^2$	$C_{44}^{(0)}$
$C_{55}=C_{44}^{(0)}+DP_S^2$	$C_{44}^{(0)}$
$C_{66}=C_{66}^{(0)}-4A^2/\Delta$	$C_{66}^{(0)}=(C_{11}^{(0)}-C_{12}^{(0)})/2$
$C_{12}=C_{12}^{(0)}+2(A^2-B^2)/\Sigma$	$C_{12}^{(0)}$
$C_{13}=C_{13}^{(0)}+2C(A-B)/\Sigma$	$C_{13}^{(0)}$
$C_{23}=C_{13}^{(0)}-2C(A+B)/\Sigma$	$C_{13}^{(0)}$

As we have already mentioned, the *z*-axis LA phonon is always a pure mode with a velocity given by $(C_{33}/\rho)^{1/2}$. On the other hand, the character of the *y*-axis LA phonon depends completely on the ferroelectric domain structure actually realized within a film. However, it is possible to show that the *y*-axis LA phonon velocity is given by a combination of the C_{11}, C_{22}, C_{12}, and C_{66} elastic constants. For example, the effective elastic constant model [13], in which the crystallographic elastic constants for each ferroelectric domain are averaged under a common weighting factor of 1/6, gives a pure LA mode with a velocity given by $[\{3(C_{11}+C_{22})+2(C_{12}+2C_{66})\}/8\rho]^{1/2}$. Since we have no information on the real ferroelectric domain structure realized within a film, let us concentrate on the C_{33} elastic constant. The electrostrictive coupling between the OP and the e_3 strain results in a step anomaly for the C_{33} elastic constant at T_c. Within the Landau framework of PTs, the electrostrictive coupling always results in a step anomaly at T_c even for second-order PTs [19]. As given in Table I, the C_{33} value below T_c should be smaller than the $C_{33}^{(0)}$ value above T_c. However, this prediction is obviously opposite to the observed temperature dependence shown in Fig. 4.

We consider the ferroelectric properties of polymers. It is well known that ferroelectric polymers are electrically very hard materials compared with the inorganic ferroelectrics, for example, $BaTiO_3$ ($T_c\sim 135\,^\circ$C), KH_2PO_4, and so on. Furukawa discussed the ferroelectric properties of P[VDF65/TrFE35] films using a standard Landau free-energy expression for a first-order PFPT [20]. He could successfully reproduce the ferroelectric properties of P[VDF65/TrFE35] films with this free energy, and found that the expansion coefficients are more than two orders of magnitude larger than those for $BaTiO_3$. With the free energy, one can readily show that the ferroelectric state in polymers stays in an extremely deep potential minimum and is very stable against external perturbations. Other important information can be deduced from the induced piezoelectricity. The induced piezoelectric strength of polymer ferroelectrics is about one order of magnitude weaker than that of $BaTiO_3$ [21]. One can readily calculate five piezoelectric constants from Eq. (7), for example, $e_{23}=2CP_S$. We have $P_S=0.115$ C/m^2 for SC 75/25 film [5] and $P_S=0.26$ C/m^2 for $BaTiO_3$ [21] at room temperature. Hence, the electrostrictive coupling constants for polymers are roughly estimated to be more than one order of magnitude smaller than those of $BaTiO_3$. Finally, one can show using Eq. (8) that the Σ term ($=\beta+2\gamma' P_S^2$) in the denominator of the elastic constants in Table I is approximately given by $\Sigma\sim|\beta'|/2$ at $T_c(=T_0+3\beta'^2/16\alpha_0\gamma')$. With these considerations and estimations, we conclude that the predicted step anomaly at T_c will be strongly suppressed by the unusually large denominator Σ which stems from the intrinsic electrical properties of polymer ferroelectrics. This conclusion may also work for the *y*-axis LA phonon. However, we should remind readers that the conclusion works only for electrostrictive coupling cases. Higher-order couplings, for example, the $D(P_x^2+P_y^2)(e_4^2+e_5^2)$ term in Eq. (7), result in a step anomaly for the transverse sound velocities due to the discontinuity of P_S^2 in Eq. (8) at T_c. Actually, Ohigashi *et al.* observed a discontinuity of sound velocity at T_c for the transverse mode that propagates along the *x* axis and is polarized along the *z* axis [7].

Another difficulty is to explain the temperature development of the phonon width shown in Figs. 3 and 4. There are two possible mechanisms that contribute to the phonon width anomaly near PTs. One is due to critical fluctuations and the other is due to the Landau-Khalatonikov process [19]. These mechanisms are generally expected to work near T_c for second-order PTs. However, in our case, the phonon widths have already started to increase even at room temperature which is about 100 °C below T_c. As already mentioned, the ferroelectric state in polymer ferroelectrics stays in an extremely deep potential minimum and is quite stable. Taking account of the strongly first-order nature of the PFPT, it is quite difficult to understand the elastic properties observed in the present BLS study by the conventional PT approaches.

B. Dispersion analysis

As a more promising approach to understanding the temperature dependence of the peak frequency and width, we consider a velocity dispersion scenario. Actually, Omote *et al.* detected two relaxations, β_c and α in their notation, from their low-frequency piezoelectric resonance study below 100 kHz [6]. A prominent change of the LA velocity along the *z* axis is associated with the β_c relaxation around $-13\,^\circ$C. The α relaxation takes place around 90 °C. Since our BLS frequencies are about five orders of magnitude higher, one can expect velocity dispersions at higher temperatures for our GHz frequencies. In order to determine relaxation parameters, we employed the viscoelastic response function given by [22]

$$S(k,\omega)\propto k_B T\frac{\Gamma''(k,\omega)}{[\omega^2-V(\omega)^2k^2+\omega\Gamma'(k,\omega)]^2+\omega^2\Gamma''(k,\omega)^2}. \tag{9}$$

Here, we have assumed that the Cole-Davidson (CD) model describes the velocity dispersion. Then, the real and imaginary parts of the memory function $\omega\Gamma(k,\omega)$ are given by

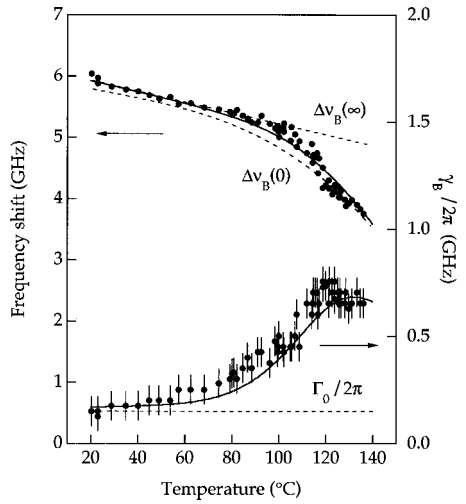

FIG. 5. Comparison between the calculated and observed peak frequency and width of the *y*-axis LA phonon as a function of temperature. The solid lines give the calculated peak frequency and width. The broken lines represent the frequencies corresponding to the limiting high- and low-frequency sound velocities and the bare width: $\Delta\nu_B(\infty)=6.11-8.9\times10^{-3}t$ GHz, $\Delta\nu_B(0)=5.9644-9.8251\times10^{-3}t+8.4255\times10^{-5}t^2-9.9242\times10^{-7}t^3$ GHz, and $\Gamma_0/2\pi=0.17$ GHz, with temperature t in °C.

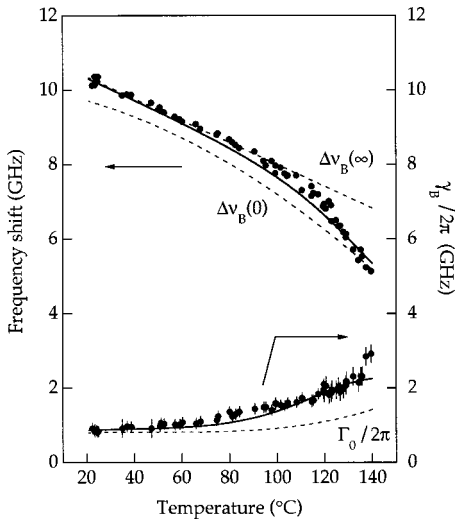

FIG. 6. Comparison between the calculated and observed peak frequency and width of the *z*-axis LA phonon. The solid lines give the calculated peak frequency and width. The broken lines are the frequencies corresponding to the limiting high- and low-frequency sound velocities and the bare width: $\Delta\nu_B(\infty)=10.95-29.5\times10^{-3}t$ GHz, $\Delta\nu_B(0)=10.031-12.257\times10^{-3}t-16.003\times10^{-5}t^2$ GHz, and $\Gamma_0/2\pi=0.81908+6.0043\times10^{-3}t-1.2373\times10^{-4}t^2+8.3173\times10^{-7}t^3$ GHz, with temperature t in °C.

$$\omega\Gamma'(k,\omega)=[V(\infty)^2-V(0)^2]k^2(\cos\psi)^{\beta_{CD}}\cos(\beta_{CD}\psi) \tag{10}$$

and

$$\omega\Gamma''(k,\omega)=\omega\Gamma_0(k,\omega)+[V(\infty)^2-V(0)^2]\times k^2(\cos\psi)^{\beta_{CD}}\sin(\beta_{CD}\psi). \tag{11}$$

Here, $V(\infty)$ and $V(0)$ are the limiting high- and low-frequency values of the sound velocity, k is the phonon momentum already defined, and $\Gamma_0(k,\omega)$ is the bare width without viscoelastic coupling. The exponent β_{CD} in Eqs. (10) and (11) takes a value between 0 and 1. We also defined the relaxation phase ψ using

$$\tan\psi=\omega\tau, \tag{12}$$

in which τ is the average relaxation time. With the response function, we repeated the numerical convolution analyses of the spectra [16]. We have five fitting parameters $V(\infty)$, $V(0)$, Γ_0, τ, and β_{CD} in Eqs. (9)–(12). We assumed a linear temperature dependence of $V(\infty)$, which can be expected from Figs. 3 and 4, and a constant value of $\beta_{CD}=0.4$. Once we determined the rest of the relaxation parameters as a function of temperature, we numerically evaluated the peak frequency and the width of the viscoelastic response function with least-squares fitted relaxation parameters to compare with the experimental values of $\Delta\nu_B$ and $\gamma_B/2\pi$ which are shown in Figs. 3 and 4.

Figure 5 shows a comparison between the experimental results and the CD analysis results for the *y*-axis LA phonon. The frequencies corresponding to the limiting velocities $[\Delta\nu_B(\infty)=\sqrt{2}V(\infty)/\lambda$ and $\Delta\nu_B(0)=\sqrt{2}V(0)/\lambda]$ and the bare width ($\Gamma_0/2\pi$) are indicated by the broken lines. The calculated peak frequency and width are shown by the solid lines. Thus the relaxation time well obeys the Arrhenius law given by

$$\tau=\tau_0\exp(\Delta E/k_BT), \tag{13}$$

in which the attempt relaxation time $\tau_0=(4.0\pm0.6)\times10^{-18}$ s and the activation energy $\Delta E=0.55\pm0.01$ eV were obtained from a least-squares fit. Note that the values of τ_0 and ΔE depend on the value of the β_{CD} exponent. We can reasonably reproduce the general trend of the observed temperature behaviors of the phonon frequency and width by the CD dispersion model. We also found that a β_{CD} exponent of 0.4–0.5 gives the best fit. We have also performed CD dispersion analyses for the *z*-axis phonon frequency and width by using the same CD response function and the relaxation time. The results are displayed in Fig. 6. However, in this case, we needed to introduce a temperature dependent bare width as shown by the broken line. For this LA phonon, we can also reproduce the general trend of the observed temperature dependence of the phonon frequency and width. In this way, the velocity dispersion model with the CD response function can reproduce the general trend of the observed temperature development of the peak frequency and width for both LA phonons. Note that the relaxation time at -13 °C is evaluated to be $\sim1.6\times10^{-7}$ s. Therefore, the BLS velocity dispersion seems to be closely related to the β_c relaxation detected by the low-frequency piezoelectric resonance study [6].

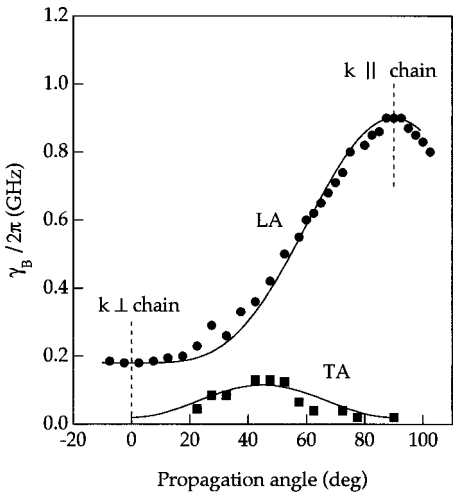

FIG. 7. Anisotropy of the in-plane phonon width as a function of the propagation angle θ at 24.0 °C. Here, θ is measured from the y axis. The solid lines are given by $\gamma_B(\theta)/2\pi = 0.18 + 0.72 \sin^4\theta$ for the LA phonon and $\gamma_B(\theta)/2\pi = 0.02 + 0.095 \sin^2 2\theta$ for the TA phonon.

C. In-plane anisotropy of phonon widths

We have examined the anisotropy of the in-plane phonon widths at 24.0 °C in the ferroelectric phase. Figure 7 shows the in-plane phonon width as a function of the phonon propagation angle θ measured from the y axis. The LA phonon width $\gamma_B/2\pi$ corresponds to the bare width $\Gamma_0/2\pi$ in our dispersion analyses at this temperature. We could not observe scattering from the transverse acoustic (TA) phonon (precisely speaking, the quasi-TA phonon) below $\theta \simeq 20°$. The solid lines, which are given by $\gamma_B(\theta)/2\pi = 0.18 + 0.72 \sin^4\theta$ for the LA phonon and $\gamma_B(\theta)/2\pi = 0.02 + 0.095 \sin^2 2\theta$ for the TA phonon, well reproduce the observed anisotropy. Krüger *et al.* reported similar but small amplitude anisotropy of the in-plane phonon widths for their P[VDF70/TrFE30] films with a lower degree of crystallinity ($\sim$60%) at 27 °C in the ferroelectric phase [23].

In order to understand the θ dependence in the ferroelectric phase, we introduce a physical quantity Q which describes a one-dimensional freedom constrained in each copolymer chain and couples to the in-plane phonons. As shown in Fig. 6, the bare LA phonon width $\Gamma_0/2\pi$ is almost independent of temperature below $\sim$100 °C, and then gradually increases through the PFPT with further increasing temperature. This temperature dependence seems to suggest that Q may not be directly related to the driving mechanism of the PFPT. It is quite interesting to note that films with a higher degree of crystallinity exhibit larger amplitude anisotropy. In such a situation, the z components of the in-plane phonon amplitudes u_z^j (j = LA and TA) and wave vector k_z effectively couple to Q. Taking account of the quasi-LA and TA characters of the in-plane phonons, we have $k_z u_z^{LA} \approx k u^{LA} \sin^2\theta$ for the LA phonon and $k_z u_z^{TA} \approx k u^{TA} \sin 2\theta/2$ for the TA phonon. The $k_z u_z^j$ (j = LA and TA) terms belong to the total symmetric A_1 representation. Since the ferroelectric C_{2v} point group possesses four one-dimensional representations, the allowed couplings between the z component of the in-plane phonons and Q are the bilinear type when Q belongs to the A_1 representation or the electrostrictive type when Q belongs to other representations. Then, renormalizing the $\sin^2\theta$ and $\sin 2\theta$ factors into the coupling constants, we have the effective coupling constants $G_{Q\text{-}LA} \sin^2\theta$ and $G_{Q\text{-}TA} \sin 2\theta$. For both bilinear and electrostrictive couplings, the lowest-order process that contributes to the width is second order, and results in the $\sin^4\theta$ and $\sin^2 2\theta$ dependence. In this way the θ dependence of the in-plane phonon widths can be understood by introducing a one-dimensional physical quantity Q.

As the most characteristic property of the SC films, Ohigashi *et al.* reported one-dimensional liquid and two-dimensional solid behavior in the paraelectric phase through their XRD, dielectric, and shear velocity investigations [7]. Their results indicate that the chain molecules, essentially composed of $TGTG'$ sequences, rapidly rotate independently of neighboring chains, and easily slip along the chain direction in the paraelectric phase. Unfortunately, the chain dynamics in the ferroelectric phase is not fully understood. Since the SC films behave as three-dimensional solids in the ferroelectric phase, the longitudinal sliding motion of the polymer chain is greatly suppressed below the PFPT. However, local sliding motion within infinitely long polymer chains of SC films can be retained in the ferroelectric phase. Q may describe such a local motion. In order to elucidate the physical meaning and dynamics of Q, we are planning detailed BLS examinations of the z-axis LA phonon at lower temperatures.

IV. CONCLUSIONS

The elastic properties of SC 75/25 films were investigated by BLS in the temperature range between 20 °C and 140 °C with increasing temperature. The in-plane LA phonons propagating parallel and perpendicular to the polymer-chain direction were examined. For both LA phonons, the phonon peak frequency exhibits a broad down-step anomaly above $\sim$100 °C, depending on the propagation direction. The width of the y-axis LA phonon exhibits a maximum centered at $\sim$120 °C. On the other hand, the width of the z-axis LA phonon continues to increase up to 140 °C through T_c, which was quite obscure in our BLS study. Furthermore, the width is unusually larger than the y-axis LA phonon width, in spite of its pure LA character.

We developed a Landau free energy to discuss the elastic properties. However, we found that the expected step anomaly at T_c from the electrostrictive coupling is strongly suppressed by the intrinsic electrical nature of polymer ferroelectrics. Instead of the PFPT approach, we applied a velocity dispersion approach using the Cole-Davidson relaxation model with an exponent of $\beta_{CD} = 0.4$. Then the relaxation time well obeys the Arrhenius law with $\tau_0 = (4.0 \pm 0.6) \times 10^{-18}$ s and $\Delta E = 0.55 \pm 0.01$ eV. With the CD relaxation model, we could reasonably reproduce the observed temperature dependence of the peak frequency and width for both LA phonons. The velocity dispersion is assigned to the β_c relaxation detected by the low-frequency piezoelectric resonance study by Omote *et al.* [6].

Finally, we have examined the anisotropy of the in-plane phonon widths at 24.0 °C in the ferroelectric phase. The anisotropy can be well described by $\gamma_B(\theta)/2\pi = 0.18 + 0.72\sin^4\theta$ for the LA phonon and $\gamma_B(\theta)/2\pi = 0.02 + 0.095\sin^2 2\theta$ for the TA phonon with the propagation angle θ measured from the y axis. The θ dependence can be explained by introducing a one-dimensional physical quantity Q. However, understanding of the physical meaning and dynamics of Q is left for future studies.

ACKNOWLEDGMENTS

This work was partly supported by a Grant-in-Aid for Scientific Research (No. 10450357) from the Ministry of Education, Science, Sports and Culture, Japan. One of the authors (A.Y.) would like to thank H. Saito, N. Ishida, S. Takahashi, H. Sato, and J.-I. Mawatari of ISU for their assistance with the experiments, and technicians in the machine shop of RISM for their collaboration in designing and assembling the oven.

[1] M. Tamura, K. Ogasawara, N. Ono, and S. Hagiwara, J. Appl. Phys. **45**, 3768 (1974).
[2] T. Furukawa, M. Date, E. Fukuda, Y. Tajitsu, and A. Chiba, Jpn. J. Appl. Phys. **19**, L109 (1980).
[3] K. Omote and H. Ohigashi, Appl. Phys. Lett. **66**, 2215 (1995).
[4] K. Omote and H. Ohigashi, IEEE Trans. Ultrason. Ferroelectr. Freq. Control **43**, 312 (1996).
[5] H. Ohigashi, K. Omote, and T. Gomyo, Appl. Phys. Lett. **66**, 3281 (1995).
[6] K. Omote, H. Ohigashi, and K. Koga, J. Appl. Phys. **81**, 2760 (1997).
[7] H. Ohigashi, K. Omote, H. Abe, and K. Koga, J. Phys. Soc. Jpn. **68**, 1824 (1999).
[8] Y. Tajitsu, M. Fujii, H. Suzuki, M. Aoki, K. Suzuki, and H. Ohigashi, Jpn. J. Appl. Phys., Part 2 **36**, L693 (1997).
[9] Y. Tajitsu, H. Ohigashi, and M. Date, J. Mater. Sci. Lett. **16**, 1378 (1997).
[10] J.K. Krüger, J. Petzelt, and J.F. Legrand, Colloid Polym. Sci. **264**, 791 (1986).
[11] J.K. Krüger, M. Prechtl, and J.F. Legrand, Ferroelectrics **109**, 315 (1990).
[12] Z. Liu and V.H. Schmidt, Ferroelectrics **119**, 9 (1991).
[13] L. Otani, J.-I. Mawatari, A. Yoshihara, and H. Ohigashi, Jpn. J. Appl. Phys., Part 1 **39**, 2922 (2000).
[14] For example, R. Jiménez, J.K. Krüger, K.-P. Bohn, and C. Fischer, J. Phys.: Condens. Matter **8**, 7579 (1996).
[15] A. Yoshihara, Jpn. J. Appl. Phys., Part 1 **33**, 3100 (1994).
[16] A. Yoshihara, H. Sato, and S. Kojima, Jpn. J. Appl. Phys., Part 1 **35**, 2925 (1996); A. Yoshihara, M. Kurosawa, and Y. Morioka, *ibid.* **36**, 3318 (1997).
[17] S. Ikeda and H. Suda, Phys. Rev. E **56**, 3231 (1997).
[18] T. Furukawa, J.X. Wen, K. Suzuki, Y. Takashina, and M. Date, J. Appl. Phys. **56**, 829 (1984).
[19] W. Rehwald, Adv. Phys. **22**, 721 (1973).
[20] T. Furukawa, Ferroelectrics **57**, 63 (1984).
[21] Y. Xu, *Ferroelectric Materials and Their Applications* (North Holland, Amsterdam, 1991).
[22] C.J. Montrose, V.A. Solovyev, and T.A. Litovitz, J. Acoust. Soc. Am. **43**, 117 (1967).
[23] J.K. Krüger, M. Prechtl, J.C. Wittmann, S. Meyer, J.F. Legrand, and G. D'Asseza, J. Polym. Sci., Part B: Polym. Phys. **31**, 505 (1993).